Self-healing hybrid nanocomposites consisting of bisphosphonated hyaluronan and calcium phosphate nanoparticles

ARTICLE *in* BIOMATERIALS · AUGUST 2014

Impact Factor: 8.56 · DOI: 10.1016/j.biomaterials.2014.05.003

Biomaterials 35 (2014) 6918–6929

Contents lists available at ScienceDirect

Biomaterials

journal homepage: www.elsevier.com/locate/biomaterials

Self-healing hybrid nanocomposites consisting of bisphosphonated hyaluronan and calcium phosphate nanoparticles

M. Reza Nejadnik [a,1], Xia Yang [b,1], Matilde Bongio [a], Hamdan S. Alghamdi [a], Jeroen J.J.P. van den Beucken [a], Marie C. Huysmans [c], John A. Jansen [a], Jöns Hilborn [b], Dmitri Ossipov [b,*], Sander C.G. Leeuwenburgh [a,*]

[a] Department of Biomaterials, Radboud University Medical Center, 6525EX Nijmegen, The Netherlands
[b] Department of Materials Chemistry, Angstrom Laboratory, A Science for Life Laboratory, Uppsala University, SE 75121 Uppsala, Sweden
[c] Department of Preventive and Restorative Dentistry, Radboud University Medical Center, 6525EX Nijmegen, The Netherlands

ARTICLE INFO

Article history:
Received 4 March 2014
Accepted 1 May 2014
Available online 24 May 2014

Keywords:
Self-healing materials
Reversible bonds
Organic-inorganic nanocomposites
Hydrogels
Bone regeneration

ABSTRACT

Non-covalent interactions are often regarded as insufficient to construct macroscopic materials of substantial integrity and cohesion. However, the low binding energy of such reversible interactions can be compensated by increasing their number to work in concert to create strong materials. Here we present the successful development of an injectable, cohesive nanocomposite hydrogel based on reversible bonds between calcium phosphate nanoparticles and bisphosphonate-functionalized hyaluronic acid. These nanocomposites display a capacity for self-healing as well as adhesiveness to mineral surfaces such as enamel and hydroxyapatite. Most importantly, these non-covalently cross-linked composites are surprisingly robust yet biodegradable upon extensive in vitro and in vivo testing and show bone interactive capacity evidenced by bone ingrowth into material remnants. The herein presented method provides a new methodology for constructing nanoscale composites for biomedical applications, which owe their integrity to reversible bonds.

1. Introduction

The irreversibility of most covalent bonds renders materials incapable of self-healing, since these bonds cannot be restored after rupture. Reversible bonds, on the other hand, are more sensitive to external stimuli and hence more appropriate for self-healing materials [1]. Nevertheless, these reversible interactions are inherently weak and often regarded as insufficient to construct macroscopic materials of substantial integrity and cohesion. In nature, however, reversible bonds are responsible for the outstanding structural properties of natural nanoscale composites such as nacre and bone. These nanocomposites owe their exceptional strength and toughness to non-covalent interactions between acidic proteins and metallic ions or inorganic nanoparticles [2,3]. As a consequence, many nanocomposites have been designed to engineer complex tissues by mimicking native nanostructures [4]. Evidently, the lower binding energy of reversible interactions can be compensated by increasing the number of these bonds to create materials with interesting functional properties [1,5–7]. Consequently, research on the use of reversible bonds to assemble smart, functional materials was intensified considerably in recent years [8–12]. Several approaches have been pursued which employ hydrogen bonds [13,14], metal-ligand coordination bonds [15,16], as well as ionic [17], hydrophobic [18,19], host–guest [20], or specific peptide–peptide interactions [21] to prepare self-healing materials. Self-healing hydrogels can be derived from either expensive amphiphilic peptides [18], engineered proteins [21], synthetic non-biodegradable polymers [13–15,20] or potentially toxic organic binders [17], but the translation of these materials towards in vivo applications in regenerative medicine is still largely unexplored.

To address the emerging need for bioresorbable hydrogels of improved functionality for regenerative medicine, we synthesized injectable, non-covalently cross-linked nanocomposites that combine self-healing and mineral-adhesive behavior with a surprising stability in vitro and in vivo by exploiting reversible bonds between calcium phosphate (CaP) nanoparticles and bisphosphonate-functionalized hyaluronan (Fig. 1a).

* Corresponding authors.
E-mail addresses: dmitri.ossipov@kemi.uu.se (D. Ossipov), sander.leeuwenburgh@radboudumc.nl (S.C.G. Leeuwenburgh).
[1] These authors contributed equally to this work.

http://dx.doi.org/10.1016/j.biomaterials.2014.05.003
0142-9612/

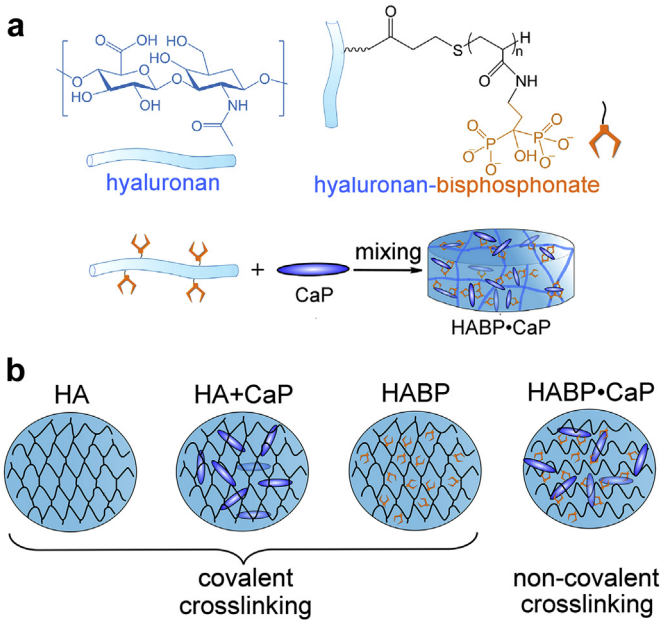

Fig. 1. Covalently and non-covalently cross-linked hyaluronan-based materials. **a)** Non-covalent cross-linking of hyaluronan-bisphosphonate by calcium phosphate (CaP) nanoparticles. **b)** Schematic representation of covalently cross-linked (HA, HA + CaP, HABP) hydrogels and non-covalently cross-linked HABP·CaP hybrid nanocomposites (for more details see Supplementary Fig. S1a).

2. Experimental section

2.1. Materials

Hyaluronidase, 8-hydroxyquinoline, O-cresolphthalein complexone (OCPC), ethanolamine, and DL-dithiothreitol were purchased from Sigma–Aldrich. $Ca(OH)_2$ and H_3PO_4 were purchased from Acros. PBS without Ca^{2+}/Mg^{2+} cations was obtained from Biochrom. 1-Ethyl-3-(3-dimethylaminopropyl)carbodiimide (EDC) and N-hydroxybenzotriazole (HOBt) were purchased from Fluka. Hyaluronan (molecular weight of 130 kDa) was purchased from Lifecore Biomedical. Dihydrazide crosslinkers 2,2′-dithiobis(ethanol-O-hydrazinocarbonyl) and disulfanediylbis (ethane-2,1-diyl)bis(2-(6-((hydrazinecarbonyl)oxy) hexanoyl) hydrazinecarboxylate) and hyaluronan-aldehyde (degree of aldehyde substitution of 5%, defined as molar ratio of aldehyde groups to hyaluronan disaccharide units) were synthesized according to a previously published protocol [22]. Acrylated bisphosphonate was prepared as described previously [23]. Initiator Irgacure® 2959 was purchased from BASF. All solvents were of analytical quality (p.a.) and dried over 4Å molecular sieves. Dialysis membranes Spectra/Por® 6 (3500 and 1000 g/mol cutoff) were purchased from VWR International.

2.2. Preparation of hyaluronan derivatives and CaP nanoparticles

2.2.1. Preparation of hyaluronan-thiol and hyaluronan-hydrazide-thiol

Hyaluronan-thiol and hyaluronan-hydrazide-thiol were synthesized according to our previously established protocol [22]. Specifically, 400 mg of hyaluronan (1 mmol of disaccharide repeating units) was dissolved in 50 mL of distilled water. For synthesis of hyaluronan-hydrazide-thiol, 23.8 mg of 2,2′-dithiobis(ethanol-O-hydrazinocarbonyl) (0.10 mmol), 92.2 mg of disulfanediylbis(ethane-2,1-diyl)bis(2-(6((hydrazinecarbonyl)oxy)hexanoyl) hydrazinecarboxylate) (0.15 mmol) and a solution of HOBt (153 mg, 1 mmol) in 5 mL of a 1:1 (v/v%) acetonitrile-water mixture were added to the hyaluronan solution. For synthesis of hyaluronan-thiol, the reaction was performed without disulfanediylbis(ethane-2,1-diyl)bis(2-(6((hydrazinecarbonyl)oxy)hexanoyl) hydrazinecarboxylate). The pH of the mixture was adjusted to 4.7 followed by addition of EDC (47.9 mg, 0.25 mmol) to the mixture, which was subsequently stirred for 20 h at room temperature. Subsequently, the pH of the reaction mixture was adjusted to 8.7 and DL-dithiothreitol (192.8 mg, 1.25 mmol) was added to the solution followed by another 20 h of stirring. Finally, the mixture was dialyzed twice against distilled, acidified water (pH 3.5) containing 0.1 M NaCl in a dialysis tube (molecular weight cutoff of 3.5 kDa). The solution was lyophilized yielding 404 mg of hyaluronan-hydrazide-thiol or 410 mg of hyaluronan-thiol. NMR experiments (δ scale; J values are in Hz) were carried out on a Jeol JNM-ECP Series FT NMR System at a magnetic field strength of 9.4 T, operating at 400 MHz. The degree of thiol substitution was verified by comparison of integration of the $-CH_2CH_2SH$ side chain peaks at 2.58 and 2.73 ppm with the acetamido moiety of the *N*-acetyl-D-glucosamine residue of hyaluronan. Comparative integration of the α, β, γ, δ, and ε methylene protons of the grafted hydrazide-terminated chains (see Fig. S1 for designation) facilitated the measurement of the degree of hydrazide substitution. ^{1}H NMR revealed that the degree of thiol substitution in both hyaluronan-hydrazide-thiol and hyaluronan-thiol was 3.1%, while the degree of hydrazide substitution in hyaluronan-hydrazide-thiol was 9.5%.

2.2.2. Synthesis of hyaluronan-bisphosphonate and hyaluronan-hydrazide-bisphosphonate

Hyaluronan-thiol and hyaluronan-hydrazide-thiol were further functionalized with bisphosphonate via thiol-ene photopolymerization as shown in Fig. S1a. To this end, various amounts of acrylated bisphosphonate were added to 400 mg of hyaluronan-thiol or hyaluronan-hydrazide-thiol in 80 mL degassed distilled water in order to obtain bisphosphonate-to-thiol molar ratios of 4:1 or 1:1. Subsequently, 8 mg of Irgacure® 2959 was added and the mixture was stirred for 10 min under ultraviolet light (36W UV timer lamp, CNC international BV, Netherlands). Thereafter, the mixture was dialyzed against 0.1 M NaCl at pH 3.5 (molecular weight cutoff of 3.5 kDa) and subsequently dialyzed against distilled water at pH 3.5 twice. The solution was neutralized to pH 7.4 and lyophilized. The resulting polymers were analyzed by ^{1}H NMR, ^{31}P NMR and elemental analysis using a colorimetric spectrophotometric method (OEA Labs). Specifically, the peaks corresponding to the native hyaluronan protons (such as acetamide protons at 1.9 ppm, 2′, 3′, 4′, 5′, and 6′-protons of the hyaluronan disaccharide unit between 3.2 and 4.0 ppm as well as anomeric 1′-protons at 4.4 ppm) were compared with peaks corresponding to the methylene protons 2 and 3 of the grafted side chains. From ^{1}H NMR data in Fig. S1b, the peak at 2.2 ppm corresponds to two methylene protons 1 that are adjacent to a bridging carbon of the bisphosphonate group.

2.2.3. Synthesis and characterization of calcium phosphate nanoparticles

A homogeneous suspension of nanosized calcium phosphate (CaP) particles was prepared according to a wet-chemical precipitation process as previously described [24]. Briefly, 25 mL of H_3PO_4 (1.78 M) solution was slowly added to a solution of continuously stirred $Ca(OH)_2$ (2.96 M) while the temperature was kept at 60 °C. The ratio between the elements was stoichiometric with respect to hydroxyapatite (Ca/P ratio of 1.67). The product was aged overnight at 60 °C, thereafter the nanoparticles were rinsed three times with milli-Q water in a series of centrifugation and re-suspension. Finally, the suspension was sonicated and the solid content was adjusted to 0.12 g/mL (corresponding to 12 w/v%). After the synthesis, the suspension containing CaP nanoparticles was subjected to wet autoclavation (121 °C in 15 min) for sterilization followed by adjustment of the pH to 7.4. Subsequently, the precipitated nanoparticles were analyzed using Attenuated Total Reflectance Fourier-Transform InfraRed spectroscopy (ATR-FTIR, Spectrum One, Perkin Elmer), X-ray Diffraction (XRD, PW 1830, Panalytical), and Transmission Electron Microscopy (TEM, JEM 1010, Jeol).

2.3. Preparation and characterization of non-covalently and covalently cross-linked formulations

Non-covalently cross-linked HABP·CaP hybrid nanocomposites were prepared by mixing equal volumes of hyaluronan-bisphosphonate with a CaP suspension in connected syringes, while three types of covalently cross-linked formulations (HA, HABP, HA + CaP) were prepared as reference compounds by mixing equal volumes of the hyaluronan derivatives as follows:

1. HA: Mixture of hyaluronan-aldehyde with hyaluronan-hydrazide (final hyaluronan content of 2 w/v%).
2. HABP: Mixture of hyaluronan-aldehyde with hyaluronan-hydrazide-bisphosphonate (final hyaluronan content of 2 w/v% hyaluronan) and degree of bisphosphonate substitution (DS_{BP}) of 8.1%.
3. HA + CaP: Mixture of hyaluronan-aldehyde with hyaluronan-hydrazide and CaP suspensions (final hyaluronan content of 2 w/v% hyaluronan and CaP content of 6 w/v%)
4. HABP·CaP: Mixture of hyaluronan-bisphosphonate with CaP suspensions (various hyaluronan and CaP contents as well as degrees of bisphosphonate substitution DS_{BP} are provided in Table 1).

This study design allowed a direct comparison of the efficacy of non-covalent BP·CaP cross-linking vs. various types of covalently cross-linked formulations.

2.3.1. Tilting test

In order to qualitatively compare the flowability of the materials, equal volumes of aqueous solutions of hyaluronan (2 w/v%), a suspension of CaP nanoparticles (6 w/v%), a mixture of hyaluronan and CaP nanoparticles (2 and 6 w/v%, respectively) and a mixture of hyaluronan-bisphosphonate and CaP nanoparticles (2 and 6 w/v%, respectively) were injected into glass vials, tilted and photographed.

2.3.2. Rheology

Rheological characterizations of the materials were performed using an AR2000 Advanced Rheometer (TA Instruments) with an aluminum parallel plate geometry of 8 mm diameter. For all rheology experiments, the total volume of

Table 1
Qualitative assessment of the consistency of non-covalently cross-linked HABP·CaP hybrid nanocomposites (at pH 7.4 in 10 mM PBS) upon variation of the concentrations of hyaluronan-bisphosphonate and CaP nanoparticles as well as the degree of bisphosphonate substitution (DS_{BP}).

Hyaluronan–bisphosphonate concentration (w/v%)	CaP nanoparticle concentration (w/v%)	DS_{BP} (mol%)	Qualitative description
0.5	6.0	8.1	Sol
1.0	6.0	8.1	Very weak gel
2.0	**6.0**	**8.1**	**Robust gel**[a]
4.0	6.0	8.1	Too viscous to be mixed
2.0	6.0	2.5	Very weak gel
2.0	6.0	30.0	Precipitate
2.0	1.5	8.1	Weak gel
2.0	3.0	8.1	Gel

[a] After optimization, non-covalently cross-linked HABP·CaP hybrids consisting of 2.0% hyaluronan-bisphosphonate (DS_{BP} of 8.1%) and 6.0% CaP nanoparticles were selected for further in vitro and in vivo tests.

tested material was 0.3 mL. After determining the linear viscoelastic regime using strain sweeps at a frequency of 1 Hz, frequency sweeps were performed by monitoring storage (G′) and loss moduli (G″) at a fixed normal force (0.03 N) and a fixed strain (1%) as a function of frequencies between 0.1 and 10 Hz. In order to investigate the self-healing capacity of the various formulations, we subjected covalently cross-linked HA + CaP (containing 2.0 w/v% hyaluronan and 6.0 w/v% CaP) and non-covalently cross-linked HABP·CaP hybrid nanocomposites (containing 2.0 w/v% hyaluronan-bisphosphonate with DS_{BP} of 8.1% and 6.0 w/v% CaP) to sequential shear strains of 1% (for 60 s), 1000% (for 30 s) and 1% (60 s) and monitored the recovery of storage (G′) and loss moduli (G″) by time sweeps at fixed frequency (1 Hz).

2.4. Adhesion to mineralized and mineral-free model surfaces

Adhesion of non-covalently cross-linked HABP·CaP hybrid nanocomposites to mineralized surfaces was performed using an AR2000 Advanced Rheometer (TA Instruments) in a pull-off mode using both synthetic CaP-coated titanium (Ti–CaP) and bovine enamel embedded in polymethylmethacrylate (PMMA-CaP) as model surfaces. Uncoated titanium and enamel-free PMMA were used as control model surfaces. CaP coatings were deposited onto commercially pure, grit-blasted titanium discs (thickness 1 mm, diameter 12 mm, average surface roughness R_a of 1.5 μm) using a commercially available radiofrequent sputter deposition system (Edwards ESM 100) as described previously using hydroxyapatite granules (CAM Bioceramics) as target materials [25]. The titanium discs were mounted on a rotating and water-cooled substrate holder at a distance between target and disc holder of 80 mm. Titanium discs were exposed to etching with argon ions for 10 min prior to sputter deposition at an argon pressure of 5×10^{-3} mbar and a sputter power of 400 W. After deposition, the CaP-coated discs were crystallized using an additional heat treatment in an infrared furnace for 30 s at 650 °C yielding 1 μm thick apatitic CaP coatings as described previously [26]. PMMA-CaP model surfaces were prepared by embedding 14–15 pieces of bovine teeth enamel at the surface of PMMA discs (Candulor AutoPlast) of 10 mm thickness and 30 mm diameter. Both model surfaces were characterized by means of thin-film X-ray diffraction (thin-film XRD, PW 1830, Panalytical) with the angle of the incident X-ray beam set at 2.5°. X-ray diffraction analysis of PMMA-CaP model surfaces (Fig. S2) revealed distinct reflection peaks characteristic of crystalline hydroxyapatite which corresponded to previously reported diffractograms for bovine enamel [27,28]. Reflection peaks as observed for Ti–CaP corresponded to apatite with a preferred orientation along the (002) plane (at 25.7 °2θ) but less intense compared to enamel in PMMA-CaP. This phenomenon can be attributed to the much lower thickness of the CaP coatings, as reflected by appearance of reflection peaks corresponding to the underlying titanium substrate.

For adhesion tests, mineralized or mineral-free model surfaces were fixed to the Peltier bottom plate and stainless steel parallel top plate geometry of 20 mm of the rheometer using double-sided carbon tape (with mineral surfaces facing the gap between both surfaces). HABP·CaP hybrid nanocomposites (containing 2.0 w/v% hyaluronan-bisphosphonate with DS_{BP} of 8.1% and 6.0 w/v% CaP) were injected on the bottom disc (0.3 mL for titanium discs and 0.4 mL for PMMA discs) and the geometry was positioned downward until the material was fully spread between the top and bottom discs. Subsequently, the experiment was started by moving the geometry upward at a rate of 50 μm/s and monitoring the normal pull-off force until a total pull-off distance of 2500 μm was reached. Pull-off stresses were calculated by dividing pull-off stresses by the surface area of the model surfaces. Three samples were measured for each experimental condition ($n = 3$) and maximum pull-off stresses were depicted as average ± standard deviation.

2.5. In vitro stability and mineralization of the hybrid nanocomposites

2.5.1. Stability in PBS or EDTA solutions

In order to test the reversibility of the interactions between calcium ions and bisphosphonate groups, HABP·CaP hybrid nanocomposites were soaked in either 10 mM PBS or ethylenediaminetetraacetic acid solution (100 mM EDTA, pH 6) and their stability was monitored for 3 h.

2.5.2. Swelling ratio

In order to study the influence of ionic strength and acidity on the swelling ratio of non-covalently cross-linked hybrid nanocomposites, HABP·CaP hydrogels (0.3 mL by volume) were immersed into 5 mL of aqueous media of either different ionic strength (distilled water, 10 mM PBS or 100 mM PBS) or pH (10 mM PBS set at pH 3.5, 5.0 or 7.4) in a glass vial. In addition, the swelling ratio of non-covalently cross-linked HABP·CaP hybrid nanocomposites was compared to the swelling of covalently cross-linked hydrogels (HA, HABP, HA + CaP) in 10 mM PBS at pH 7.4. All measurements were repeated three times ($n = 3$). For all swelling experiments, the mass of the each wet sample (W_w) was measured after 1, 4, 8, and 24 h. Finally, the samples were lyophilized to obtain the dry weights (W_d). The swelling ratio (%) was calculated according to the formula: Swelling ratio $= ((W_w - W_d)*100)/W_d$

2.5.3. Enzymatic degradation

Enzymatic degradation of covalently cross-linked (HA + CaP) and non-covalently cross-linked (HABP·CaP) nanocomposites was compared quantitatively by immersing 300 μL of each sample into either 3 mL PBS or Simulated Body Fluid (SBF, containing 136.8 mM NaCl, 3 mM KCl, 1.5 mM $MgCl_2$, 2.5 mM $CaCl_2$, 1 mM K_2HPO_4, 4.15 mM $NaHCO_3$ and 0.5 mM Na_2SO_4) [29]. Both PBS and SBF buffers contained 5 UI/mL of hyaluronidase to facilitate enzymatic degradation of hyaluronan macromers. Every 24 h for up to 120 h, the supernatants were collected and freeze-dried prior to measurement of the weight, while 3 mL of either (hyaluronidase-containing) PBS or SBF were added again to maintain a constant supernatant volume. All experiments were repeated three times ($n = 3$). The degradation rate was presented as the weight loss relative to the original sample mass.

2.5.4. Mineralization in vitro

The mineralization behavior of non-covalently cross-linked HABP·CaP hybrid nanocomposites and covalently cross-linked HA, HA + CaP and HABP formulations was compared quantitatively by immersing 200 μL of sample in 12-well plates filled with 4 mL of freshly prepared, filter-sterilized Simulated Body Fluid (ionic composition as described above) [29]. Three empty wells were also filled with SBF (control). The plates were kept at 37 °C while shaking moderately (60 rpm). The SBF was changed every 4 days (up to 20 days), and the supernatant was collected to determine calcium concentrations using the ortho-cresolphthalein complexone (OCPC, Sigma–Aldrich) method. To this end, 100 μL of the supernatant was mixed with 100 μL of 1 N acetic acid and incubated overnight on a shaking table. Mineralization of the hyaluronan-based hydrogels was calculated from the cumulative uptake of calcium from SBF (relative to the controls) and depicted as average ± standard deviation for three samples per group ($n = 3$).

2.6. In vivo performance of the hybrid nanocomposites

2.6.1. Implant preparation for in vivo study

For the animal implantation study, a total of four hyaluronan-based hydrogels were implanted into both bone and subcutaneous tissue of rats, i.e., three covalently cross-linked hydrogels (i.e. HA, HA + CaP, HABP) and one non-covalently cross-linked hybrid (HABP·CaP) (Fig. 1b). The hyaluronan content was 2.0 w/v% for all formulations while the CaP content and DS_{BP} were fixed at 6.0 w/v% (for HA + CaP and HABP·CaP) and 8.1% (for HABP and HABP·CaP), respectively. The two components of each formulation were loaded in two separate 1.0 mL BD Luer-Lock™ disposable syringes (Becton Dickinson) followed by mixing 50 times (left-right) prior to surgery. For subcutaneous implantation, translucent inserts for 24-well plates (Greiner-Bio One) were used as molds to cast pre-made, cylindrical formulations one day prior to surgical implantation. First, the bottom layer (i.e. film) of each insert was removed, whereafter 200 μl of sample was injected. Samples were obtained prior to surgery by extrusion from the top of these inserts.

2.6.2. Surgical procedure

A total of twenty-four healthy, skeletally mature male Wistar rats (mean body weight: 350 g) were used. Before experimentation, animal procedures were evaluated and approved by the Animals Ethics Committee of the Radboud University Nijmegen, the Netherlands (DEC 2011-279). Furthermore, the specifications of the approved institutional ethical protocol were followed (CDL-90155) and all procedures were performed according to ISO-standards (ISO 9001:2008). Animals were housed in pairs for a 7-day acclimatization period prior to surgery. A bilateral frontal femoral condyle defect and two subcutaneous implantations were performed in each animal (Fig. S3, $n = 6$ per experimental group per time point). General anesthesia was induced and maintained by inhalation of isoflurane/N_2O/O_2 (Rhodia Organique Fine Limited). To minimize postoperative pain, Rimadyl® (5.0 mg/kg, Pfizer Animal Health) was administered subcutaneously before surgery. Buprenorfine (0.02 mg/kg; Temgesic®, Reckitt Benckiser Health Care Limited) was

provided for additional analgesia before surgery and two times a day for two days post surgery.

Prior to injection of hyaluronan-based hydrogels into the femoral condyles, rats were immobilized in a supine position and the hind limbs were shaved and disinfected with povidone-iodine. A parapatellar, longitudinal incision was made on the medial surface of the condyle to avoid cutting into the patellar tendon. The knee joint capsule was then incised longitudinally, and the patellar tendon was gently moved laterally to expose the knee joint. At the femoral intercondylar notch, a cylindrical defect with a diameter of 2.85 mm and a depth of 3.0 mm was created in the same direction of the long axis of the femur. Specifically, the defects in the femora were drilled with an increasing burr diameter (from 2.0 mm to 2.85 mm) using a low-speed dental drilling system (800 rpm, Elcomed 100, W&H Dentalwerk Burmoos) and continuous external cooling with saline. The drilled cavity was then washed with saline and packed using cotton gauzes soaked with lidocaine (with 1:100.000 epinephrine (1 w/v%), Fresenius Kabi, Den Bosch, the Netherlands) to minimize bleeding. After complete drying of the defect, the needle (0.8 diameter, 21G) connected to the syringe loaded with one of the four hyaluronan-based formulations was positioned onto the bottom of the defect followed by injection of the hyaluronan-based formulations with simultaneous retrograde withdrawal of the needle until complete filling of the defect was reached. Subsequently, the patellar tendon was put back into place with a slight extension of the knee, and the soft tissue layers and skin overlying the defect were closed with resorbable sutures (Vicryl® 4.0, Ethicon Products). For placement of pre-set subcutaneous implants, rats were immobilized in the prone position followed by shaving of the dorsum and disinfection with povidone-iodine. A full-thickness skin incision of approximately 1.5 cm was made on each side of the vertebral column. Subsequently, a subcutaneous pocket was created laterally to the incisions using blunt dissection with scissors. One pre-set formulation was placed in each pocket and the skin was closed using staples (Agraven®, Instruvet). After surgery, the animals were housed in pairs and given access to water and food ad libitum. Moreover, animals were physically examined at regular intervals with specific focus on body weight, infections and proper mobility. The rats were euthanized by CO_2/O_2-suffocation in groups of twelve at 1 and 4 weeks after implantation.

2.6.3. Specimen retrieval and histological preparation

Following euthanasia, subcutaneously implanted formulations including surrounding tissue as well as femoral condyles were harvested and used for histomorphometric analysis that provides reliable information on bone formation as well as the tissue quality. Samples were fixed in 10% phosphate-buffered formalin solution (pH = 7.4). After 2 days, the specimens were dehydrated in a graded series of ethanol (from 70% to 100%). Subcutaneously implanted hydrogels were cut in half and embedded in paraffin. Subsequently, histological sections (6 μm thickness) were stained with hematoxylin and eosin. Femoral condyles were embedded in methylmethacrylate for polymerization. Thin sections (±8 μm) were prepared in a cross-sectional direction perpendicular to the long axis of the femur using a saw microtome with a diamond blade (SP 1600, Leica Microsystems). At least three histological sections for each specimen were obtained from the central part of the implant and stained with methylene blue and basic fuchsin.

2.6.4. Histological and histomorphometrical evaluation

Sections of both subcutaneous scaffolds and femoral condyles were imaged using light microscopy (Axio Imager Microscope Z1, Carl Zeiss Micro imaging GmbH) followed by a qualitative evaluation of the material appearance and tissue response. Since the presence of CaP nanoparticles complicated quantification of new bone formation using microcomputed tomography, the quantitative evaluation of new bone formation was performed using light microscopy within a pre-defined region of interest, which was set by positioning a circular area with a diameter equal to the final drill. Identification of bone tissue was based on both color (from staining) and morphology. Within the region of interest, the newly-formed bone was scored using a computer-based image analysis technique (Leica® Qwin Pro-image analysis) and expressed relative to the total area of the region of interest. Statistical analysis was performed with GraphPad Instat version 3.06 (GraphPad Software, San Diego CA, USA) using a one-way ANOVA combined with a post-hoc Tukey–Kramer Multiple Comparisons Test. Differences were considered statistically significant at a p-value less than 0.05.

3. Results and discussion

3.1. Design of hybrid, non-covalently cross-linked nanocomposites

Crystalline hydroxyapatite nanoparticles and hyaluronan were selected as dispersed matrix composite components since hydroxyapatite is the main mineral phase in bone tissue while hyaluronan is abundantly present in the extracellular matrix of connective tissues. Consequently, hyaluronan is currently used in clinics as a viscoelastic filler [30], and injectable formulation for treatment of arthritis [31] and as a drug delivery vehicle [32], whereas CaP ceramics have become the synthetic material of choice to stimulate bone regeneration [33–35].

Bisphosphonates are the most commonly prescribed drugs to treat osteoporosis and exhibit an exceptionally strong affinity to the mineral CaP phase in bone [36,37]. Although bisphosphonates form strong coordination bonds with a range of metallic cations including calcium [38], their calcium-binding capacity has never been exploited for the design of non-covalently cross-linked nanocomposite materials. Recent insights on the interaction between bisphosphonates and precipitated nanocrystalline apatite surfaces indicated that the binding between bisphosphonate and calcium ions induces protonation and subsequent solubilization of orthophosphate ions from the apatite surface [39]. It was concluded that bisphosphonates cannot only associate with calcium ions, but also replace orthophosphate ions from apatitic surfaces, thereby ensuring a tight interaction with crystalline solids. Hence, we hypothesized that the covalent attachment of bisphosphonate groups to the polymer backbone of hyaluronan can facilitate the formation of a hybrid nanocomposite based on reversible incorporation of polymer-grafted bisphosphonate ligands into CaP nanoparticles. In this way, release of free bisphosphonates to the surrounding physiological environment and associated biological effects on osteoclasts were expected to be minimal, although potential medicinal effects of conjugated bisphosphonates cannot be ruled out yet and should be investigated in future in vitro and in vivo studies.

3.2. Preparation of hyaluronan derivatives and CaP nanoparticles

We functionalized hyaluronan with bisphosphonate groups via thiol-ene photopolymerization [40] between acrylated aminobisphosphonate [41] and a thiol-modified hyaluronan [41,42] to obtain water-soluble hyaluronan-bisphosphonate (Fig. S1a). Variation of the bisphosphonate-to-thiol ratio allowed tuning of the degree of bisphosphonate substitution (DS_{BP} – defined as the molar ratio of bisphosphonate groups to hyaluronan disaccharide units) which ranged between 2.5% and 30% as determined by elemental analysis (Table 1). This elemental analysis also revealed that the DS_{BP} was 8.1% and 2.5% for polymers prepared at a bisphosphonate-to-thiol ratio of 4:1 or 1:1, respectively. Since the initial degree of thiol substitution was 3.1% as measured by ^{1}H NMR, the actual bisphosphonate-to-thiol molar ratio after the thiol-ene addition reaction should be 0.8:1 for the initial (acrylated) bisphosphonate-to-thiol ratio of 1:1, and 2.6:1 for the initial (acrylated) bisphosphonate-to-thiol ratio of 4:1. This indicates that at a low initial bisphosphonate-to-thiol ratio of 1:1, only 2.48% of the thiol groups reacted with acrylated bisphosphonate, while the remaining 0.62% of the thiol groups were eliminated from the thiol-ene addition through a side disulfide cross-linking reaction. At a high initial bisphosphonate-to-thiol ratio of 4:1, all thiol groups were modified with an average of 2.6 bisphosphonate groups linked to each thiol group. It has been reported that addition of thiol to vinyl monomers proceeds via a step growth mechanism [40], resulting in addition of one monomer molecule per thiol group. However, carbon radical propagation was also observed after initial thiyl radical addition to acrylate monomers leading to a chain growth [43]. Hence, it was possible to link more than one bisphosphonate group per thiol group on hyaluronan polymers. ^{31}P NMR showed a single peak at 18.9 ppm which confirmed attachment of bisphosphonate groups to hyaluronan (Fig. S1c). However, the bisphosphonate intensity for the hyaluronan derivative with DS_{BP} 2.5% was too low to be detected by ^{31}P NMR. Hence, we could only observe the peak for the derivatives with DS_{BP} 8.1%.

To compare the gelation and stability of non-covalently cross-linked HABP·CaP hybrid nanocomposites with conventional

covalently cross-linked hyaluronan hydrogels (Fig. 1b), additional hyaluronan derivatives were synthesized by single functionalization with either hydrazide (hyaluronan-hydrazide, degree of hydrazide substitution was 9.5%) or aldehyde (hyaluronan-aldehyde, degree of aldehyde substitution was 5%) [22], or dual functionalization with hydrazide and bisphosphonate (hyaluronan-hydrazide-bisphosphonate, degrees of hydrazide and bisphosphonate substitutions were 9.5% and 8.1%, respectively). ^{1}H and ^{31}P NMR analysis confirmed the successful synthesis of hyaluronan-bisphosphonate and hyaluronan-hydrazide-bisphosphonate derivatives (Fig. S1b and c).

Nanosized CaP particles were synthesized using an established wet-chemical neutralization reaction between calcium hydroxide and phosphoric acid [24,44]. The apatitic nature of the prepared nanoparticles was confirmed by XRD analysis. Main reflection peaks were observed at 25.9° and 31.9° 2θ corresponding to an apatitic CaP phase (Fig. S4a). Corresponding ATR-FTIR analyses showed that the nanoparticles consisted of hydroxyapatite with clear phosphate absorption peaks at 563, 601, 963, and 1027 cm^{-1} and a hydroxyl absorption peak at 630 cm^{-1} (Fig. S4b). From representative TEM images, the average diameter and length of the needle-shaped nanoparticles were estimated to be around 20 nm and 80 nm, respectively (Fig. S4c).

3.3. Preparation and characterization of non-covalently and covalently cross-linked hydrogels

Non-covalently cross-linked HABP·CaP hybrid nanocomposites were prepared by simple mixing of hyaluronan-bisphosphonate with CaP nanoparticles. For reasons of comparison, three conventional, covalently cross-linked hydrogels were prepared by mixing i) hyaluronan-hydrazide with hyaluronan-aldehyde (forming HA; hydrazone cross-linked hyaluronan hydrogel) [41,42], ii) CaP nanoparticles with hyaluronan-hydrazide and hyaluronan-aldehyde (forming HA + CaP; hydrazone cross-linked hyaluronan-CaP composite hydrogel), and iii) hyaluronan-hydrazide-bisphosphonate with hyaluronan-aldehyde (forming HABP; hydrazone cross-linked hyaluronan hydrogel with covalently grafted BP groups). The hydrazone cross-linking density was kept equal for all covalently cross-linked hydrogels (HA, HA + CaP and HABP). Fig. 2 shows a schematic representation of all experimental groups.

An initial qualitative confirmation of our hypothesis regarding the use of bisphosphonate·CaP interactions was obtained upon mixing of hyaluronan-bisphosphonate and CaP nanoparticles, which resulted in instantaneous formation of HABP·CaP hybrid nanocomposites containing 2 w/v% hyaluronan-bisphosphonate (DSBP = 8.1%) and 6 w/v% CaP nanoparticles. Simple tilting tests confirmed that bisphosphonate moieties were responsible for this phenomenon, since a mixture of 2 w/v% hyaluronan and 6 w/v% CaP nanoparticles was still flowable similar to a solution of 2 w/v% hyaluronan-bisphosphonate or a suspension of 6 w/v% CaP nanoparticles (Fig. S5). Scanning electron microscopy of HABP·CaP nanocomposites revealed that single CaP particles were homogeneously dispersed throughout the organic matrix (Fig. S6h). We varied the number of interactions between bisphosphonate groups and calcium ions on the surface of CaP nanoparticles by systematic variation of the solid content of hyaluronan and CaP nanoparticles as well as the degree of bisphosphonate substitution in order to tune the consistency of the resulting hybrid nanocomposites (Table 1). At the highest bisphosphonate substitution degree (i.e. 30%), precipitation was observed without any sign of gel formation due to excessive agglomeration of CaP nanoparticles. At lower bisphosphonate substitution degrees (i.e. 8.1 or 2.5%), hydrogel nanocomposites were obtained ranging from mechanically robust to very weak gels or sols.

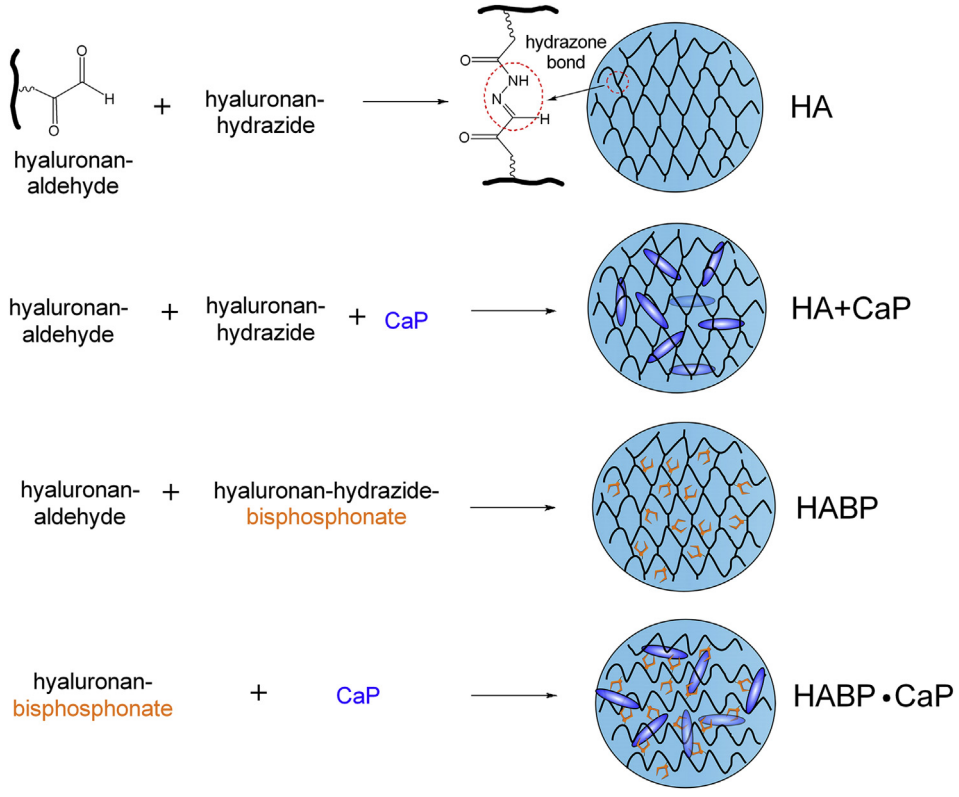

Fig. 2. Schematic representation of covalently cross-linked (HA, HA + CaP, HABP) and non-covalently cross-linked hydrogels (HABP·CaP).

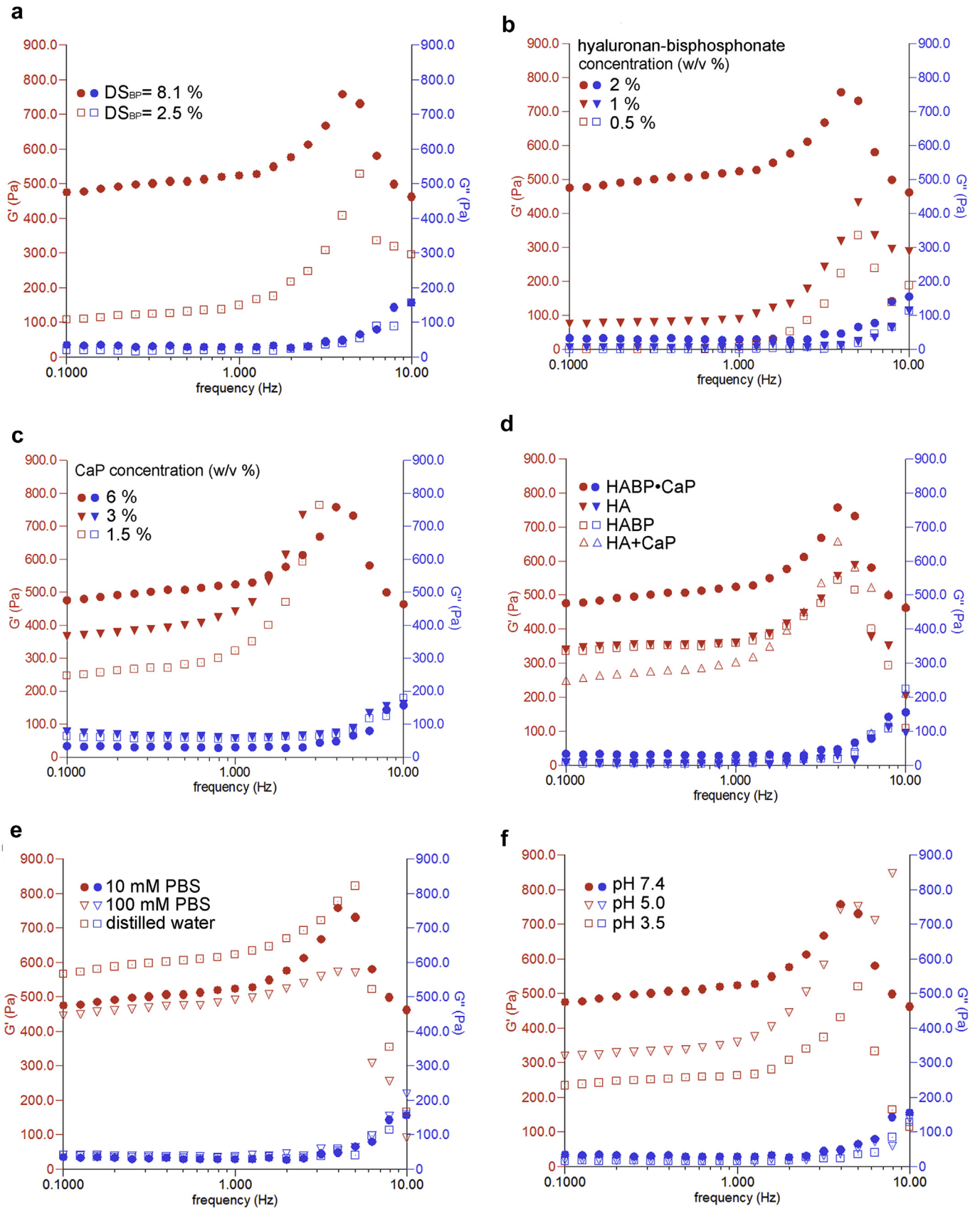

Fig. 3. Frequency sweeps of: **a)** non-covalently cross-linked HABP·CaP hybrids as a function of degree of bisphosphonate substitution (DS_{BP}) (hyaluronan-bisphosphonate polymer concentration = 2 w/v%, CaP concentration = 6 w/v%), **b)** HABP·CaP hybrids as a function of hyaluronan-bisphosphonate polymer concentration (DSBP = 8.1%, CaP concentration = 6 w/v%), **c)** HABP·CaP hybrids as a function of CaP nanoparticle concentration (hyaluronan-bisphosphonate polymer concentration = 2 w/v%, DSBP = 8.1%), **d)** HABP·CaP hybrids as compared to covalently cross-linked hyaluronan hydrogels (HA, HABP, HA + CaP), **e)** HABP·CaP hybrids as a function of ionic strength, and f) HABP·CaP hybrids as a function of pH.

3.3.1. Rheological analysis

The qualitative observations on the formation of hybrid nanocomposites were confirmed quantitatively by rheological analysis of HABP·CaP hybrid nanocomposites as a function of hyaluronan and CaP nanoparticle concentrations as well as bisphosphonate substitution degree. Frequency sweeps showed that liquid-like behavior (characterized by storage modulus G′ lower than loss modulus G″) was only observed at a low polymer concentration of 0.5 w/v% hyaluronan-bisphosphonate. The storage modulus increased i) five-fold by increasing the bisphosphonate substitution degree from 2.5 to 8.1%, ii) hundred-fold by increasing the hyaluronan-bisphosphonate content from 0.5 to 2.0 w/v%, and iii) two-fold by increasing the CaP content from 1.5 to 6.0 w/v% (Fig. 3a–c), emphasizing that the number of interactions between CaP and bisphosphonate was critical for the formation of HABP·CaP hybrid nanocomposites.

After optimizing the absolute and relative amounts of the organic and inorganic composite components and the degree of bisphosphonate substitution, the most stable formulation contained 2 w/v% hyaluronan-bisphosphonate ($DS_{BP} = 8.1\%$) and 6 w/v % CaP nanoparticles. This formulation was selected to study the viscoelastic, self-healing and mineral-adhesive properties of HABP·CaP hybrid nanocomposites in comparison to three covalently cross-linked hyaluronan-based hydrogels as controls (Fig. 1b). Notably, the HABP·CaP nanocomposites revealed higher storage moduli than any of the covalently cross-linked hyaluronan-based hydrogels with or without CaP nanoparticles (Fig. 3d). The addition of CaP nanoparticles decreased the storage modulus of covalently cross-linked hyaluronan hydrogels, indicating that the covalent cross-linking between hydrazide and aldehyde groups was compromised by CaP nanoparticles. In contrast, CaP nanoparticles were shown to be essential for the gel formation and stiffness of non-covalently cross-linked HABP·CaP hybrid nanocomposites caused by the formation of strong yet reversible bonds between CaP and bisphosphonate ligands that – when acting in concert – appeared to be stronger than the chemical network of hydrazone cross-links. Storage moduli of non-covalently cross-linked HABP·CaP nanocomposites decreased only moderately with increasing ionic strength (Fig. 3e), but the effect of pH decrease on hydrogel nanocomposite stiffness was more pronounced, as evidenced by a two-fold lower storage modulus at pH 3.5 (Fig. 3f). These results confirmed that charge screening affected the bond strength between grafted bisphosphonate groups and CaP nanoparticles only weakly, while the stability of non-covalently cross-linked nanocomposites was obviously compromised by protonation of the phosphonate groups and partial dissolution of CaP nanoparticles.

Further, non-covalently cross-linked HABP·CaP displayed superior self-healing behavior compared to covalently cross-linked

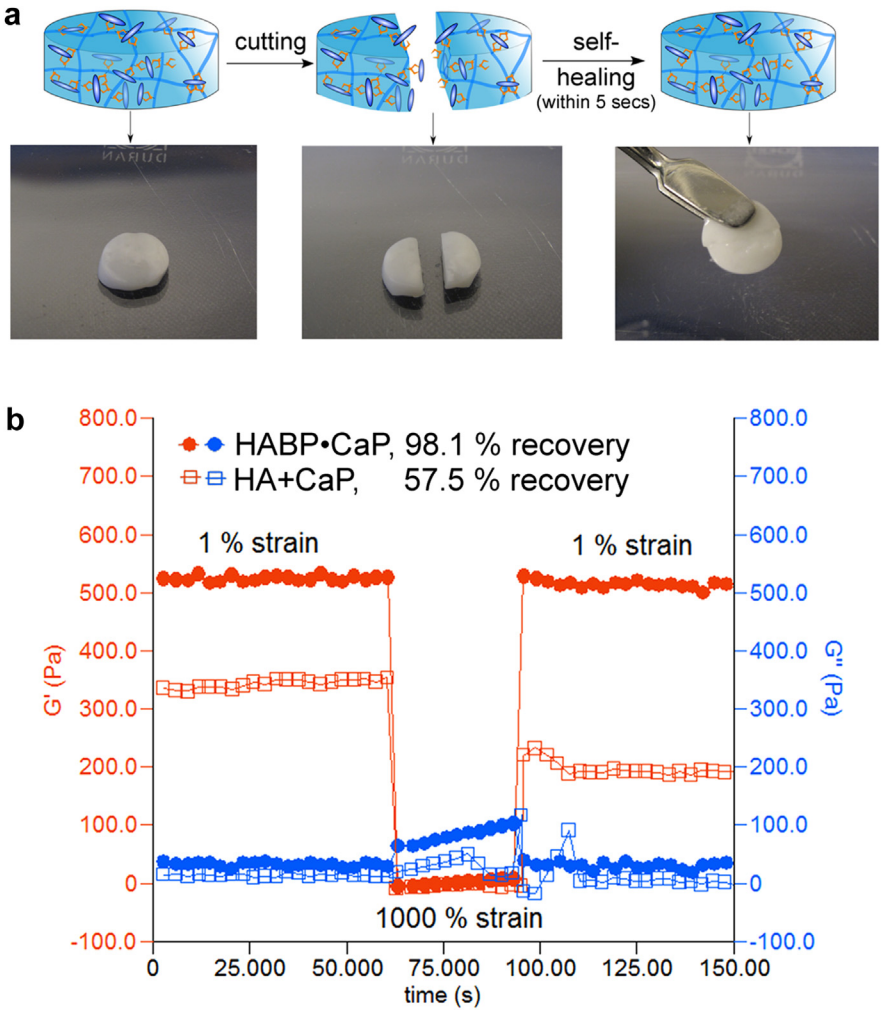

Fig. 4. Self-healing behavior of non-covalently cross-linked HABP·CaP hybrid nanocomposites containing 2 w/v% hyaluronan-bisphosphonate (DSBP = 8.1%) and 6 w/v% CaP nanoparticles. **a)** Schematic illustration and photographs of self-healing after failure induced by cutting. **b)** Recovery of non-covalently cross-linked HABP·CaP and covalently cross-linked HA + CaP hydrogels after sequential shear strains of 1%, 1000% and 1%.

hyaluronan hydrogels, confirming the potential of employing reversible bonds between grafted bisphosphonate groups and calcium phosphate nanoparticles. Following failure by cutting cylindrical hydrogels, HABP·CaP hybrids showed recovery of cohesiveness within less than 5 s (Fig. 4a and Video S1), whereas covalently cross-linked analogs containing equal amounts of CaP nanoparticles (HA + CaP) did not heal. In order to quantify this self-healing behavior, the storage and loss modulus of both covalently cross-linked (HA + CaP) and non-covalently cross-linked (HABP·CaP) nanocomposites were measured upon application of sequential strains of 1%, 1000% and 1% (Fig. 4b). Both hydrogels displayed liquid-like behavior at high strain (i.e. $\tan\delta > 10$), but the storage modulus of non-covalently cross-linked HABP·CaP nanocomposite recovered instantaneously and almost completely (98%), whereas covalently cross-linked HA + CaP nanocomposite recovered only partially (57%). This self-healing behavior is most likely attributed to fast and reversible restoration of broken bonds between bisphosphonate moieties conjugated to hyaluronan and calcium cations as present at the surface of hydroxyapatite nanoparticles. Since bisphosphonate groups were recently shown to substitute for orthophosphate ions on CaP surfaces [39], we speculate that the bond between hyaluronan-bisphosphonate and CaP was stronger than other less specific non-covalent interactions, such as interactions between carboxylate groups of hyaluronan and CaP or hydrophobic interactions. As a result, compared to other non-covalently cross-linked gels [15,45], recovery of HABP·CaP was more rapid and pronounced. This self-healing behavior does not render HABP·CaP hybrid nanocomposites suitable for load-bearing applications. Nevertheless, recovery of gel elasticity after severe shearing could be beneficial in terms of clinical handling since extrusion from medical syringes in minimally invasive surgical procedures should not compromise gel cohesiveness (see Fig. S7 and Video S2).

Supplementary video related to this article can be found at http://dx.doi.org/10.1016/j.biomaterials.2014.05.003.

3.4. Mineral adhesion testing

Besides promoting the internal cohesion of nanocomposites, functionalization of hyaluronan with bisphosphonate groups rendered HABP·CaP nanocomposites adhesive to external mineral surfaces (CaP-coated titanium and tooth enamel embedded in PMMA; Fig. S2), since a cohesive failure mode was observed after pulling-off non-covalently cross-linked HABP·CaP nanocomposites from both mineral surfaces. In contrast, adhesive failure at the interface was observed after pulling-off HABP·CaP nanocomposites from mineral-free surfaces, i.e. titanium and PMMA (Fig. 5a and b). Monitoring the stresses (as generated by HABP·CaP nanocomposites upon retracting both mineral and mineral-free surfaces from each other) revealed that considerable stresses were developed by bisphosphonate-containing nanocomposites, but not by mixtures of bisphosphonate-free hyaluronan and CaP nanoparticles (Fig. 5c). Maximum pull-off forces generated by HABP·CaP nanocomposites from mineral surfaces were more than two-fold higher compared to mineral-free control surfaces (Fig. 5d). Apparently, the surface density of bisphosphonate groups in HABP·CaP nanocomposites was sufficiently high to establish strong yet reversible interactions between bisphosphonate groups and the calcium ions as present in external hydroxyapatite surfaces.

3.5. In vitro stability and mineralization

To investigate the chemical nature of the cross-linking in more detail, the stability of non-covalently cross-linked HABP·CaP hybrid nanocomposites was tested in vitro as a function of soaking time in

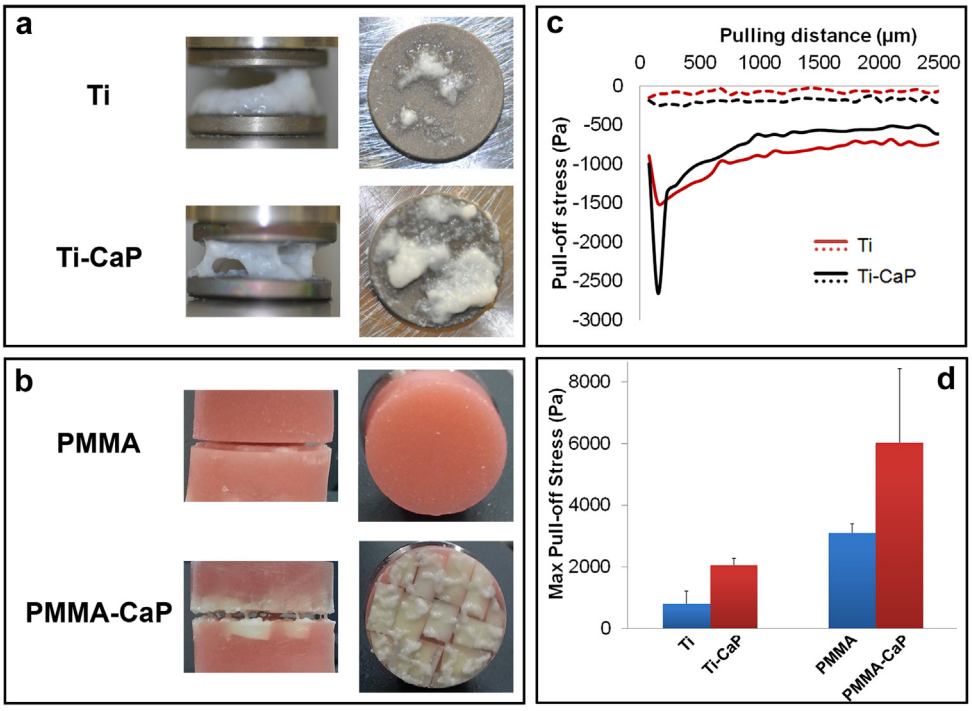

Fig. 5. Mineral adhesion of non-covalently cross-linked HABP·CaP hybrid nanocomposites containing 2 w/v% hyaluronan-bisphosphonate (DSBP = 8.1%) and 6 w/v% CaP nanoparticles. **a)** Side- and top-views after pulling-off HABP·CaP from uncoated titanium (Ti) and hydroxyapatite-coated titanium (Ti–CaP) surfaces. **b)** Side- and top-views after pulling-off HABP·CaP from polymethylmethacrylate (PMMA) and PMMA containing embedded bovine teeth (PMMA-CaP). **c)** Representative pull-off stresses for HABP·CaP hybrid nanocomposites (continuous lines) and mixtures of bisphosphonate-free hyaluronan with CaP nanoparticles (dotted lines). **d)** Maximum pull-off stresses for HABP·CaP hybrids from mineralized (Ti–CaP, PMMA-CaP) and mineral-free surfaces (Ti, PMMA); error bars indicate the standard deviation.

10 mM Phosphate Buffered Saline (PBS) or a 100 mM solution of ethylenediaminetetraacetic acid (EDTA, pH 6), which is a well-known chelating agent for calcium ions. Non-covalently cross-linked HABP·CaP nanocomposites were dissolved completely within 3 h of soaking in EDTA solution (Fig. S8) which confirmed that the gelation was based on the interaction between bisphosphonate groups grafted to hyaluronan and CaP nanoparticles. The HABP·CaP nanocomposites were, however, stable in PBS (Fig. S8). They swelled substantially in water, while change of ionic strength and pH of the buffered solution affected their swelling behavior only to a little extent (Fig. 6a and b). Swelling of HABP·CaP nanocomposite hydrogel was similar to the swelling behavior of the covalently cross-linked counterparts in 10 mM PBS at pH 7.4 (Fig. 6c). As such, it was shown in vitro that CaP nanoparticles can act as non-covalent cross-linkers for bisphosphonate-functionalized polymers without the need for additional covalent -and potentially cytotoxic- cross-linking.

Enzymatic degradation of non-covalently cross-linked HABP·-CaP nanocomposites depended on the presence of calcium ions in aqueous media since degradation was faster in calcium-free PBS compared to calcium-containing Simulated Body Fluid, a solution containing physiological concentrations of the most important ions in serum (Fig. 6d). Degradation of covalently cross-linked hydrogels, on the other hand, was similar in PBS and SBF. These results indicate that the dynamic equilibrium between bisphosphonate groups and calcium ions can be shifted toward the formation of reversible, network-stabilizing bonds by providing more calcium in aqueous media, whereas irreversible, covalent hydrazone bonds are not affected by the presence of calcium ions.

Bisphosphonate groups grafted to hyaluronan also stimulated mineralization in vitro. Upon prolonged soaking of both covalently (HA, HA + CaP, HABP) and non-covalently cross-linked (HABP·-CaP) formulations in SBF, we observed that HABP·CaP mineralized most extensively (Fig. S9). The calcium uptake by plain hyaluronan hydrogels was negligible (irrespective of the bisphosphonate substitution degree), indicating that mineralization was mainly induced by CaP nanoparticles. Quantification of the calcium uptake by covalently cross-linked HA + CaP nanocomposites was complicated by premature release of CaP nanoparticles from the hyaluronan matrix, which suggests a lack of interaction between the bisphosphonate-free organic matrix and dispersed nanoparticles.

3.6. In vivo stability

The above-described in vitro experiments confirmed that reversible bonds between CaP nanoparticles and bisphosphonate-functionalized hyaluronan induce sufficient non-covalent cross-linking of HABP-CaP nanocomposites to warrant stability upon prolonged soaking in SBF. Nevertheless, we questioned whether

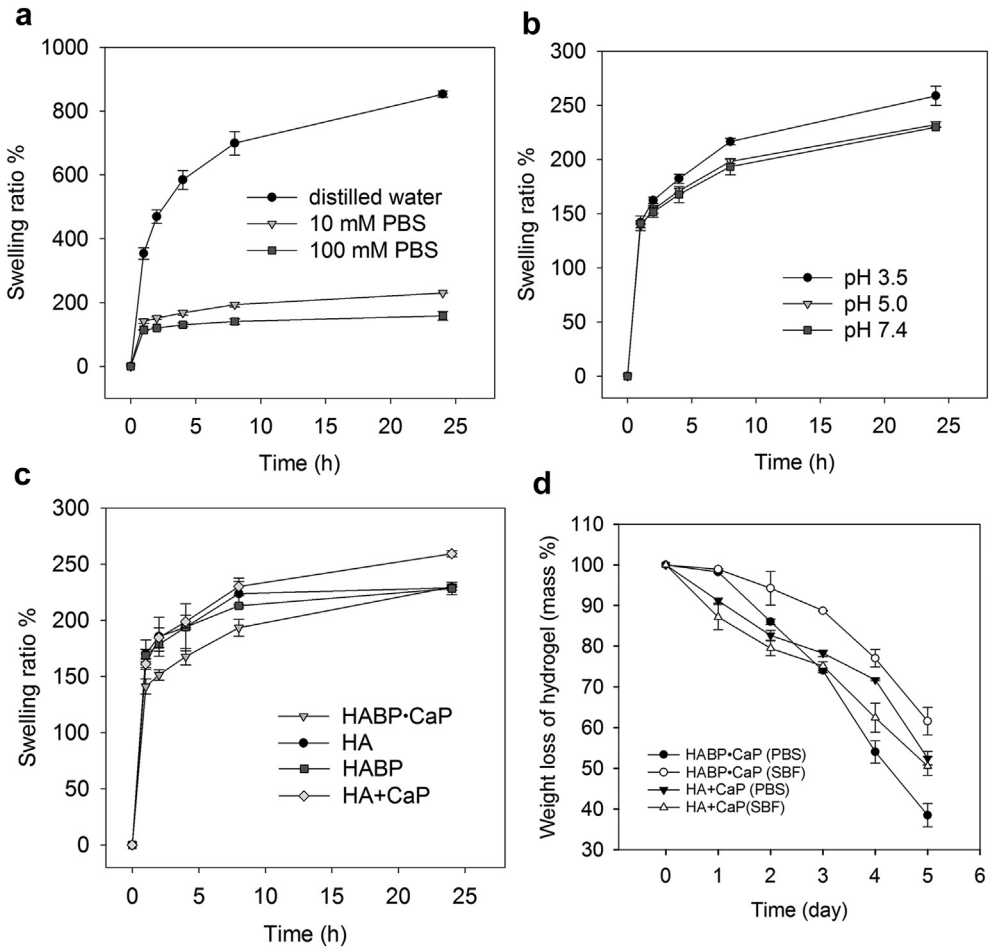

Fig. 6. Swelling ratio of non-covalently cross-linked HABP·CaP hybrid nanocomposites (containing 2 w/v% HABP (DS_{BP} = 8.1%) and 6 w/v% CaP nanoparticles) **a)** as a function of ionic strength at pH 7.4 ($n = 3$), **b)** as a function of pH in 10 mM PBS ($n = 3$), **c)** compared to covalently cross-linked hydrogels (HA, HABP, HA + CaP) in 10 mM PBS at pH 7.4 ($n = 3$), **d)** as a function of enzymatic degradation time compared to covalently cross-linked HA + CaP composites in either PBS or Simulated Body Fluid (pH 7.4 and hyaluronidase concentration of 5 UI/mL) ($n = 3$).

this non-covalent cross-linking would be sufficiently strong to withstand the highly dynamic in vivo conditions. Consequently, both covalently (HA, HA + CaP, HABP) and non-covalently cross-linked hydrogels (HABP·CaP) were implanted subcutaneously and in a bone defect in rats (see Fig. S3 for implantation models) followed by evaluation of material performance after 1 and 4 weeks. Subcutaneously, the covalently cross-linked formulations and non-covalently cross-linked HABP·CaP retained their original shape after 1 week implantation. However, the distribution of CaP nanoparticles became heterogeneous within covalently cross-linked hyaluronan (HA + CaP) while remaining homogeneous within non-covalently cross-linked HABP·CaP hybrid nanocomposites (Fig. S10). Pronounced degradation and cell infiltration were observed particularly for bisphosphonate-free materials (HA and HA + CaP) after 4 weeks of subcutaneous implantation (Fig. 7a–d), whereas materials containing bisphosphonated hyaluronan (HABP and HABP·CaP) retained their original size as well as microstructure, and were surrounded by a thin fibrous capsule of ~10 layers of elongated fibroblasts (Fig. 7e and g). Although cells infiltrated these materials peripherally, no cells were observed in central regions of the implants (Fig. 7f and h). This observation indicates that the bisphosphonate groups and their interaction with calcium ions or CaP nanoparticles stabilized hyaluronan more efficiently in vivo than hydrazone cross-links. For the

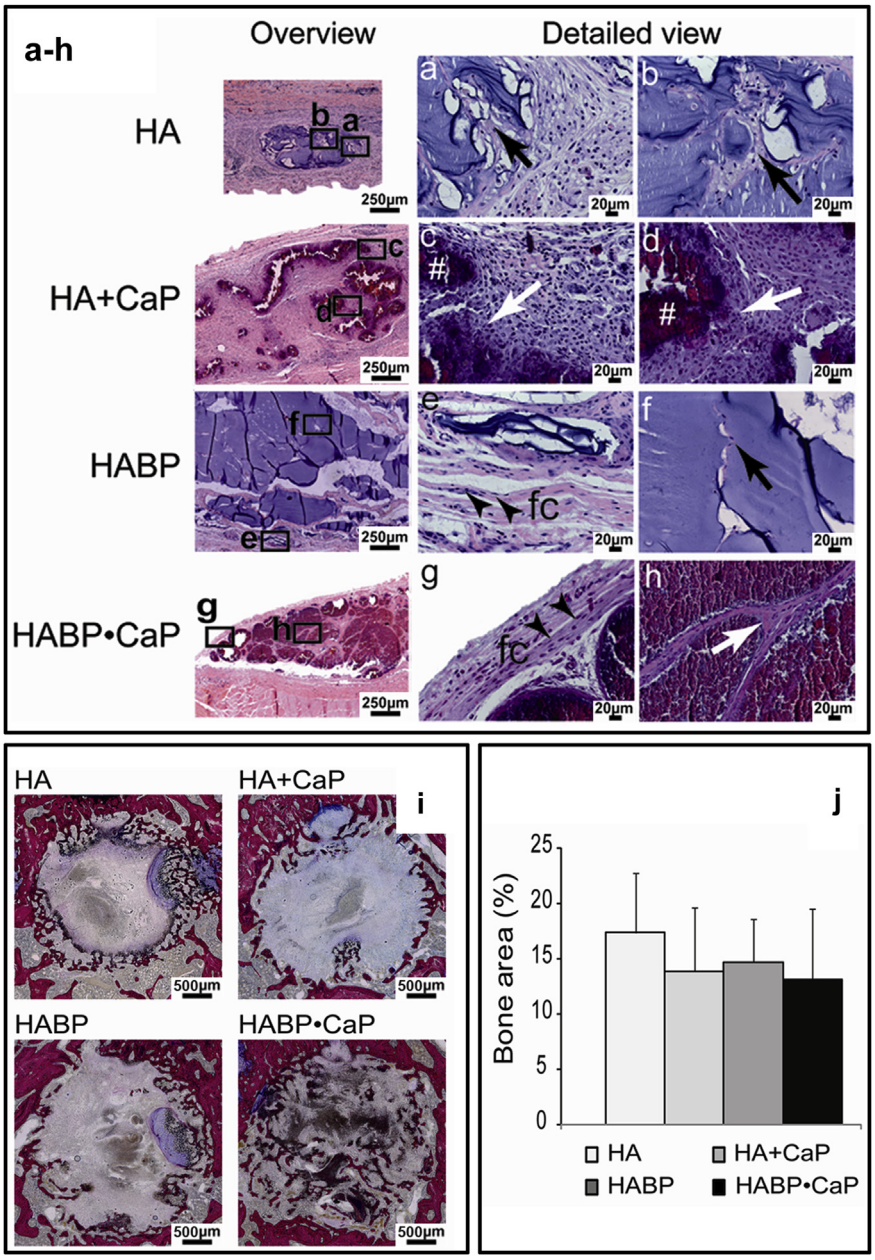

Fig. 7. Stability of non-covalently vs. covalently cross-linked hyaluron-based formulations after four weeks of implantation in subcutaneous (a–h) and bone tissue (i, j). **a)** Abundant peripheral cell infiltration in HA. **b)** Abundant central cell infiltration in HA. **c)** Abundant peripheral cell infiltration in HA + CaP. **d)** Abundant central cell infiltration in HA + CaP. **e)** Fibrous capsule around HABP. **f)** Poor cell infiltration in HABP. **g)** Fibrous capsule around HABP·CaP. **h)** Poor cell infiltration in HABP·CaP. Arrows indicate infiltrating cells, # indicates CaP-enriched area, fc indicates fibrous capsule, arrowheads indicate fibroblasts. **i)** Histology of covalently (HA, HABP, HA + CaP) and non-covalently (HABP·CaP) cross-linked formulations after 4 weeks of implantation in bone tissue. **j)** Bone regeneration after 4 weeks of implantation; error bars indicate the standard deviation.

HABP·CaP hybrid nanocomposites, the direct interaction of bisphosphonate to CaP nanoparticles preserved the homogeneous distribution of the nanoparticles, limited the infiltration of cells within the polymeric matrix, and retained the integrity of the scaffolds.

Similar degradation behavior was observed for the various formulations injected in bone defects. Histological analysis after 1 week revealed that the bone defects were always completely filled with the materials. New bone formation was only observed at the material–bone interfaces (Fig. S11). Abundant bone formation was observed after 4 weeks, with covalently cross-linked materials (HA, HA + CaP and HABP) displaying new bone formation at the edges of the defect, whereas non-covalently cross-linked HABP·CaP hybrid nanocomposites showed newly-formed trabecular-like bone homogeneously interspersed throughout the material (Fig. 7i). We speculate that the HABP·CaP hybrid nanocomposites exhibited a more homogeneous nanostructure the covalently cross-linked materials, which resulted into a more stable environment for attachment of osteoprogenitor cells and a more homogeneous biodegradation behavior. CaP nanoparticles stabilized by reversible bonds with bisphosphonate groups seemed to act as nanometer-sized seeds which supported bone conduction. Specifically, aggregates of calcified matrix (bone spicules) started to develop throughout the bone defect in direct apposition to remnants of HABP·CaP hybrid nanocomposites as well as bone trabecula (Fig. S12). Quantification of the amount of newly-formed bone confirmed that non-covalently cross-linked HABP·CaP nanocomposites were as biodegradable as various covalently cross-linked hydrogels without provoking any adverse tissue response such as inflammation (Fig. 7j). Apparently, the reversible bonds between bisphosphonate groups and CaP nanoparticles were sufficiently strong to preserve the distribution of the CaP nanoparticles within the hyaluronan matrix and retain the integrity of the nanocomposite in vivo even in the absence of irreversible, covalent cross-links between hyaluronan macromers.

4. Conclusions

We have presented a non-covalently cross-linked hybrid nanocomposite, which outperforms conventional, covalently cross-linked analogs in terms of self-healing capacity as well as adhesiveness to mineral surfaces. Most importantly, these non-covalently cross-linked composites were surprisingly robust yet biodegradable upon extensive in vitro and in vivo testing, thereby confirming that cohesive nanocomposites can be developed based on reversible bonds between polymer-grafted bisphosphonate ligands and calcium ions as present on the surface of nanoscale inorganic particles. The biological observation that a hydrogel based on such reversible bonds aids in the progression of bone formation throughout the material is particularly appealing for bone regenerative applications.

Acknowledgments

We acknowledge financial support from 1) the SmartMix Program (TeRM project) of the Netherlands Ministry of Economic Affairs and Ministry of Education; 2) Culture and Science, Netherlands; 3) European Community's Seventh Framework Programme (MultiTERM, Grant no: 238551).

Appendix A. Supplementary data

Supplementary data related to this article can be found at http://dx.doi.org/10.1016/j.biomaterials.2014.05.003.

References

[1] Rybtchinski B. Adaptive supramolecular nanomaterials based on strong noncovalent interactions. Acs Nano 2011;5(9):6791–818.
[2] Fantner GE, Hassenkam T, Kindt JH, Weaver JC, Birkedal H, Pechenik L, et al. Sacrificial bonds and hidden length dissipate energy as mineralized fibrils separate during bone fracture. Nat Mater 2005;4(8):612–6.
[3] Suzuki M, Saruwatari K, Kogure T, Yamamoto Y, Nishimura T, Kato T, et al. An acidic matrix protein, Pif, is a key macromolecule for nacre formation. Science 2009;325(5946):1388–90.
[4] Dvir T, Timko BP, Kohane DS, Langer R. Nanotechnological strategies for engineering complex tissues. Nat Nanotechnol 2011;6(1):13–22.
[5] Cordier P, Tournilhac F, Soulie-Ziakovic C, Leibler L. Self-healing and thermoreversible rubber from supramolecular assembly. Nature 2008;451(7181):977–80.
[6] Dankers PYW, Harmsen MC, Brouwer LA, Van Luyn MJA, Meijer EW. A modular and supramolecular approach to bioactive scaffolds for tissue engineering. Nat Mater 2005;4(7):568–74.
[7] Schmuck C. Supramolecular structures robust materials from weak forces. Nat Nanotechnol 2011;6(3):136–7.
[8] Appel EA, Loh XJ, Jones ST, Biedermann F, Dreiss CA, Scherman OA. Ultrahigh-water-content supramolecular hydrogels exhibiting multistimuli responsiveness. J Am Chem Soc 2012;134(28):11767–73.
[9] Haque MA, Kurokawa T, Kamita G, Gong JP. Lamellar bilayers as reversible sacrificial bonds to toughen hydrogel: hysteresis, self-recovery, fatigue resistance, and crack blunting. Macromolecules 2011;44(22):8916–24.
[10] Imato K, Nishihara M, Kanehara T, Amamoto Y, Takahara A, Otsuka H. Self-healing of chemical gels cross-linked by diarylbibenzofuranone-based trigger-free dynamic covalent bonds at room temperature. Angew Chem Int Ed 2012;51(5):1138–42.
[11] Krieg E, Weissman H, Shirman E, Shimoni E, Rybtchinski B. A recyclable supramolecular membrane for size-selective separation of nanoparticles. Nat Nanotechnol 2011;6(3):141–6.
[12] Wang HA, Hansen MB, Lowik DWPM, van Hest JCM, Li YB, Jansen JA, et al. Oppositely charged gelatin nanospheres as building blocks for injectable and biodegradable gels. Adv Mater 2011;23(12):H119–24.
[13] Cui JX, del Campo A. Multivalent H-bonds for self-healing hydrogels. Chem Commun 2012;48(74):9302–4.
[14] Phadke A, Zhang C, Arman B, Hsu CC, Mashelkar RA, Lele AK, et al. Rapid self-healing hydrogels. P Natl Acad Sci USA 2012;109(12):4383–8.
[15] Holten-Andersen N, Harrington MJ, Birkedal H, Lee BP, Messersmith PB, Lee KYC, et al. pH-induced metal-ligand cross-links inspired by mussel yield self-healing polymer networks with near-covalent elastic moduli. P Natl Acad Sci USA 2011;108(7):2651–5.
[16] Zhou YX, Sharma N, Deshmukh P, Lakhman RK, Jain M, Kasi RM. Hierarchically structured free-standing hydrogels with liquid crystalline domains and magnetic nanoparticles as dual physical cross-linkers. J Am Chem Soc 2012;134(3):1630–41.
[17] Wang Q, Mynar JL, Yoshida M, Lee E, Lee M, Okuro K, et al. High-water-content mouldable hydrogels by mixing clay and a dendritic molecular binder. Nature 2010;463(7279):339–43.
[18] Hamley IW. Self-assembly of amphiphilic peptides. Soft Matter 2011;7(9):4122–38.
[19] Yao HB, Tan ZH, Fang HY, Yu SH. Artificial nacre-like bionanocomposite films from the self-assembly of chitosan-montmorillonite hybrid building blocks. Angew Chem Int Ed 2010;49(52):10127–31.
[20] Kakuta T, Takashima Y, Nakahata M, Otsubo M, Yamaguchi H, Harada A. Preorganized Hydrogel: self-healing properties of supramolecular hydrogels formed by polymerization of host-guest monomers that contain cyclodextrins and hydrophobic guest groups. Adv Mater 2013;25(20):2849–53.
[21] Parisi-Amon A, Mulyasasmita W, Chung C, Heilshorn SC. Protein-engineered injectable hydrogel to improve retention of transplanted adipose-derived stem cells. Adv Healthc Mater 2013;2(3):428–32.
[22] Ossipov DA, Piskounova S, Varghese OP, Hilborn J. Functionalization of hyaluronic acid with chemoselective groups via a disulfide-based protection strategy for in situ formation of mechanically stable hydrogels. Biomacromolecules 2010;11(9):2247–54.
[23] Wang L, Zhang M, Yang ZM, Xu B. The first pamidronate containing polymer and copolymer. Chem Commun 2006;26:2795–7.
[24] Nejadnik MR, Mikos AG, Jansen JA, Leeuwenburgh SCG. Facilitating the mineralization of oligo(poly(ethylene glycol) fumarate) hydrogel by incorporation of hydroxyapatite nanoparticles. J Biomed Mater Res A 2012;100A(5):1316–23.
[25] Wolke JGC, van der Waerden JPCM, Schaeken HG, Jansen JA. In vivo dissolution behavior of various RF magnetron-sputtered Ca-P coatings on roughened titanium implants. Biomaterials 2003;24(15):2623–9.
[26] Yoshinari M, Hayakawa T, Wolke JGC, Nemoto K, Jansen JA. Influence of rapid heating with infrared radiation on RF magnetron-sputtered calcium phosphate coatings. J Biomed Mater Res 1997;37(1):60–7.
[27] Yoshida Y, Yoshihara K, Nagaoka N, Hanabusa M, Matsumoto T, Momoi Y. X-ray diffraction analysis of three-dimensional self-reinforcing monomer and its chemical interaction with tooth and hydroxyapatite. Dent Mater J 2012;31(4):697–702.

[28] Yoshihara K, Yoshida Y, Hayakawa S, Nagaoka N, Irie M, Ogawa T, et al. Nanolayering of phosphoric acid ester monomer on enamel and dentin. Acta Biomater 2011;7(8):3187–95.
[29] Kokubo T, Takadama H. How useful is SBF in predicting in vivo bone bioactivity? Biomaterials 2006;27(15):2907–15.
[30] Fakhari A, Berkland C. Applications and emerging trends of hyaluronic acid in tissue engineering, as a dermal filler and in osteoarthritis treatment. Acta Biomater 2013;9(7):7081–92.
[31] Colen S, van den Bekerom MPJ, Mulier M, Haverkamp D. Hyaluronic acid in the treatment of knee osteoarthritis a systematic review and meta-analysis with emphasis on the efficacy of different products. Biodrugs 2012;26(4):257–68.
[32] Prestwich GD. Hyaluronic acid-based clinical biomaterials derived for cell and molecule delivery in regenerative medicine. J Control Release 2011;155(2):193–9.
[33] Chai YC, Carlier A, Bolander J, Roberts SJ, Geris L, Schrooten J, et al. Current views on calcium phosphate osteogenicity and the translation into effective bone regeneration strategies. Acta Biomater 2012;8(11):3876–87.
[34] Troczynski T. Bioceramics – a concrete solution. Nat Mater 2004;3(1):13–4.
[35] Yuan HP, Fernandes H, Habibovic P, de Boer J, Barradas AMC, de Ruiter A, et al. Osteoinductive ceramics as a synthetic alternative to autologous bone grafting. P Natl Acad Sci USA 2010;107(31):13614–9.
[36] Boanini E, Gazzano M, Rubini K, Bigi A. Composite nanocrystals provide new insight on alendronate interaction with hydroxyapatite structure. Adv Mater 2007;19(18):2499.
[37] Russell RGG. Bisphosphonates: the first 40 years. Bone 2011;49(1):2–19.
[38] Queffelec C, Petit M, Janvier P, Knight DA, Bujoli B. Surface modification using phosphonic acids and esters. Chem Rev 2012;112(7):3777–807.
[39] Pascaud P, Gras P, Coppel Y, Rey C, Sarda S. Interaction between a bisphosphonate, tiludronate, and biomimetic nanocrystalline apatites. Langmuir 2013;29(7):2224–32.
[40] Cramer NB, Davies T, O'Brien AK, Bowman CN. Mechanism and modeling of a thiol-ene photopolymerization. Macromolecules 2003;36(12):4631–6.
[41] Yang X, Akhtar S, Rubino S, Leifer K, Hilborn J, Ossipov D. Direct "click" synthesis of hybrid bisphosphonate-hyaluronic acid hydrogel in aqueous solution for biomineralization. Chem Mater 2012;24(9):1690–7.
[42] Yang X, Kootala S, Hilborn J, Ossipov DA. Preparation of hyaluronic acid nanoparticles via hydrophobic association assisted chemical cross-linking-an orthogonal modular approach. Soft Matter 2011;7(16):7517–25.
[43] Reddy SK, Okay O, Bowman CN. Network development in mixed step-chain growth thiol-vinyl photopolymerizations. Macromolecules 2006;39(25):8832–43.
[44] Kumar R, Prakash KH, Cheang P, Khor KA. Temperature driven morphological changes of chemically precipitated hydroxyapatite nanoparticles. Langmuir 2004;20(13):5196–200.
[45] Haines-Butterick L, Rajagopal K, Branco M, Salick D, Rughani R, Pilarz M, et al. Controlling hydrogelation kinetics by peptide design for three-dimensional encapsulation and injectable delivery of cells. P Natl Acad Sci USA 2007;104(19):7791–6.